Hindawi
Advances in Civil Engineering
Volume 2023, Article ID 8854624, 20 pages
https://doi.org/10.1155/2023/8854624

Research Article

2d Models of Steel Beams under Patch Loading for Buckling Coefficient Assessment

Emanuele Maiorana,[1] **Angelo Aloisio**,[2] **and Bruno Briseghella**[3]

[1]*Department of Civil, Chemical, Environmental, and Material Engineering, University of Bologna, Viale Risorgimento 2, Bologna, Italy*
[2]*Department of Civil, Construction-Architectural and Environmental Engineering, Università degli Studi dell'Aquila, Piazzale Pontieri 1, Monteluco di Roio, L'Aquila, Italy*
[3]*College of Civil Engineering, Fuzhou University, Fuzhou, China*

Correspondence should be addressed to Angelo Aloisio; angelo.aloisio1@univaq.it

Received 20 August 2023; Revised 17 October 2023; Accepted 24 October 2023; Published 22 November 2023

Academic Editor: Federico Gusella

This paper proposes an equivalent 2d model incorporating translational and rotational springs to simulate constraints in the stability analysis of steel plates under in-plane patch loading. The main objective is to develop an equivalent stability analysis of these plates by accurately calibrating the level of constraint provided by the stiffeners and flanges. The calibration involves determining the spring constants of a 2d equivalent plate model to achieve the same linear elastic critical load and buckled shape as a 3d model. The paper uses the buckling coefficient as the objective function to calibrate the translational and rotational springs. The ultimate goal is to effectively replicate the constraint conditions imposed by the flanges and vertical stiffeners within the structure. The proposed simplified method yields results that closely align with those obtained from the original 3d model, incorporating finite-rigidity restraints.

1. Introduction

The structural analysis of steel beams subjected to patch loading is crucial for ensuring their stability and performance. Traditional approaches often involve complex and computationally expensive three-dimensional (3d) finite element (FE) models, which accurately capture the complex behavior of the system. However, such models can be time-consuming and challenging to implement in the practical design.

Longitudinal and transverse elements, such as flanges and stiffeners, are commonly used to enhance the elastic critical load for stability. Numerous studies [1–6] have contributed to the existing literature on panel stiffening. The eigenbuckling problem, often approached through closed-form solutions or numerical methods, is widely employed to analyze plates subjected to uniform axial load, bending moment, and shear [7, 8]. Various analytical, experimental, and numerical investigations have explored elastic and plastic mechanisms [6, 9, 10] and the impact of tolerances and imperfections on elastic critical loads and ultimate resistance values [11, 12].

Moreover, studies have examined specific scenarios, such as the effects of holes on plate behavior [13–16], patch loading [11, 17, 18], and local symmetrical loads and shear on perforated plates [19]. Experimental works on plates subjected to local loads are relatively limited, and no evaluation has been performed to assess the confinement effect of the elastic constraints, which is the primary focus of this research. In [20], Gozzi analyzed the model for patch loading resistance referred to in EN 1993-1-5. From the parametric numerical study with a focus on the load length, he concluded that (s_s) should follow the recommendations in EN 1993-1-5, i.e., for several loading plates, the center-to-center distance between the outermost plates plus the load spread through the plates should be used. Kovesdi et al. [21] performed numerical parametric investigations of loading length influence on patch loading resistance of girders with corrugated webs. The authors concluded that the load-carrying capacity increases nearly linearly with increasing loading length.

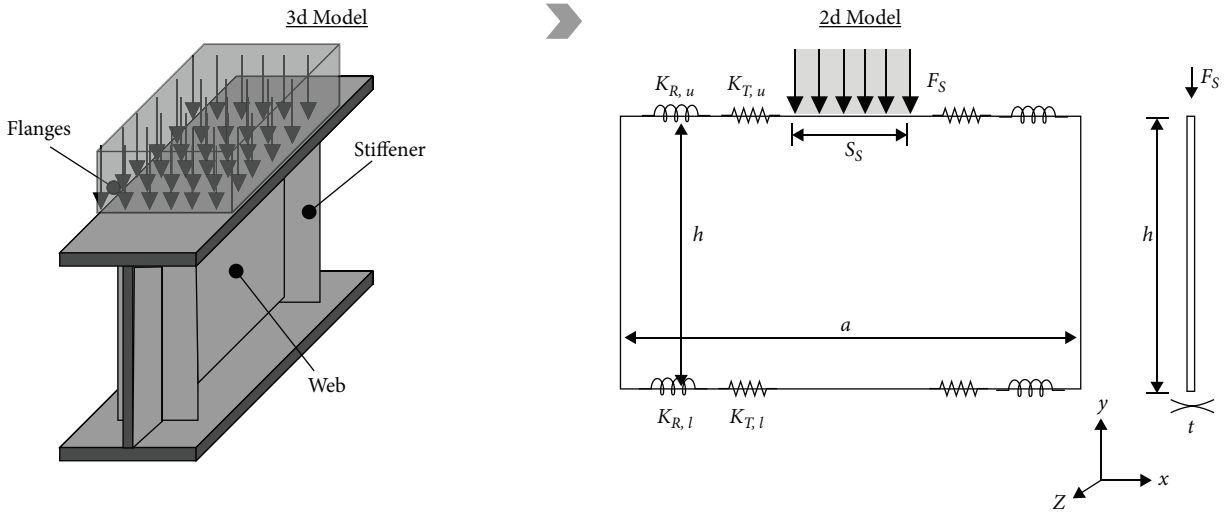

FIGURE 1: Transition from the 3d beam model to the equivalent 2d plate model.

Despite the advancements in the field [22–25], there is still a gap in the literature regarding the calibration and estimation of equivalent stiffness parameters for 2d models tailored explicitly for steel beams subjected to patch loading. This paper addresses this gap by presenting a methodology for calibrating an FE model and estimating the equivalent stiffness parameters of 2d models. Additionally, this research extends the investigation by considering the influence of patch load length on the resistance of I-girders, as studied by Rogač et al. [18]. By leveraging recent advancements in the field and building upon the existing body of the literature, this research contributes to the ongoing efforts to enhance the stability analysis of steel beams in the practical design applications.

The novelty of this research lies in developing a comprehensive approach that allows engineers to estimate the buckling coefficient using simplified 2d models efficiently. The methodology begins with calibrating a 2d FE model against 3d FE data and establishing analytical solutions to ensure accuracy and reliability. The equivalent 2d models represent a compromise between capturing the essential characteristics of the 3d beam and simplifying the analysis process. By judiciously selecting the appropriate stiffness parameters, such as translational and rotational spring constants, the 2d models can adequately mimic the behavior of the 3d beam under patch-loading conditions.

The contributions of this research are significant in terms of practicality and efficiency. The estimated stiffness parameters of the equivalent 2d models allow engineers to perform rapid and reliable buckling coefficient assessments for steel beams.

2. Problem Formulation and Methodology

This study focuses on establishing correlations between the geometry of elements that confine a double I-shaped girder and the degree of constraints applied to the web panel by flanges and vertical stiffeners for stability analysis. The FE method is employed to achieve this, utilizing the Strand7 code developed by G+D computing [26]. Translational and rotational spring elements are used to represent these constraints. The determination of the spring constants denoted as K, is based on the stiffness contributed by the surrounding elements relative to the web panel of the beam. The analysis considers the upper and lower flanges of equal size and the transverse vertical stiffeners.

In subsequent numerical analyses involving variations in geometrical shape and patch load length, the ultimate objective is establishing a calibration law for the translational and rotational springs. This calibration law is determined through linear eigenbuckling analyses, aiming to numerically obtain an identical buckling coefficient, denoted as k_{cr}, in both the comprehensive 3d model, which encompasses the web/flanges/stiffeners system, and the simplified 2d plate model that represents an elastically constrained panel (Figure 1).

The proposed calibration law aims to consistently and accurately represent the structural behavior by the simplified 2d equivalent plate model. This will significantly reduce the computational complexity compared to the comprehensive 3d model while maintaining high accuracy.

2.1. Problem Formulation. Linear buckling analyses are performed to determine the value of the theoretical and critical load. Starting from the condition of simple support, increasing values of rotational stiffness of the constraints are adopted. The constraints are implemented through rotational springs parallel to the sides of the plate, with a constant rotational stiffness K_R (N·mm/rad) along the entire perimeter of the plate. To normalize this parameter, the rotational stiffness per unit length ($K'_R = \frac{K_R \cdot n_{KR}}{a}$), where a is the web width and n_{KR} is the number of constrained nodes on each side) is divided by the flexural stiffness of the plate to obtain the dimensionless term $K_{R,\mathrm{rel}}$:

$$K_{R\mathrm{rel}} = \frac{K_R \cdot n_{KR} \cdot 12(1-\nu^2) \cdot h}{E \cdot t^3 a}, \tag{1}$$

where ν is the Poisson's coefficient, h is the height of the web, t the web thickness, and E is the Young's modulus. The adopted comparison term is the buckling coefficient k_{cr},

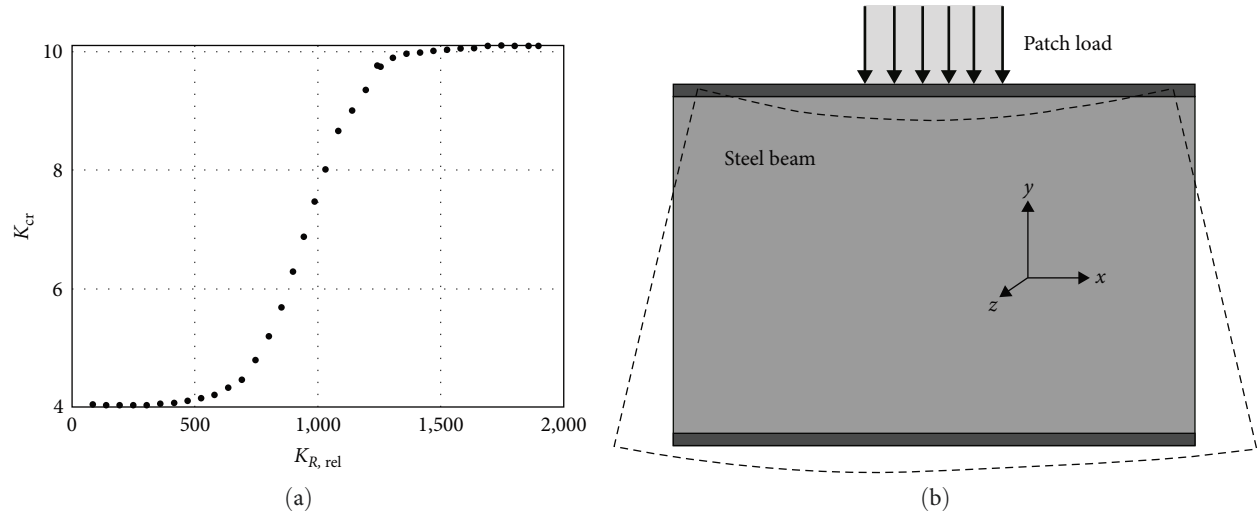

FIGURE 2: (a) k_{cr} vs. $K_{R,rel}$ for rectangular plate under uniform compression load; (b) deformed and undeformed geometries.

which is determined as follows [7]:

$$k_{cr} = \frac{\lambda_1 \cdot \sigma_0 \cdot 12(1-\nu^2) \cdot h^2}{\pi^2 \cdot E \cdot t^2}, \tag{2}$$

where λ_1 is the first eigenvalue and σ_0 is compression stress in the plate.

The solution for a square and multiple rectangular plates with simple support and uniform compressive load is $k_{cr} = 4$ [7]. Figure 2 shows the increase in the buckling coefficient as the degree of constraint increases from simple support to fixed support. The elastic constant of the spring thus has a range of variability between these two extremes.

The stabilizing effect provided by increasing the value of rotational stiffness is demonstrated by the fact that a panel, free to rotate at the perimeter ($k_{R,rel} = 0$), exhibits a reduced resistance to buckling (low k_{cr} values). Conversely, the same plate clamped on all sides ($k_{R,rel} = \infty$) yields a critical load value more than double ($k_{cr} > 10$). Configurations exist between these two extreme cases where $k_{R,rel}$ assumes a finite stiffness value, resulting in a progressive increase in the critical load. The elastic constraints are calibrated based on the buckling coefficient. Under the same applied load, achieving the same eigenvalue and instability mode is necessary through a linear stability analysis of the models. The outcome is an elastically constrained plate model that ensures an equivalent resistance to instability as flanges and stiffeners bound the web panel. Figure 2(b) illustrates an equivalent 2d model of the web. The load acts symmetrically for the width without any eccentricity concerning the web plane. The ends of the upper and lower flanges can move longitudinally along the x-axis symmetrically, while displacements in the vertical direction (Δz) out of the plane are prevented. To avoid instability and for symmetry reasons, the constraint in the x-direction is placed on the axis of symmetry at the locations of the two flanges. Vertical displacements along the y-axis are prevented along the two vertical sides to simulate the effect of the remaining part of the beam and ensure that symmetric shear forces balance the load.

2.2. Methodology. The transition from the 3d to the 2d plate model requires careful consideration of the interaction between components, such as the web, flanges, and stiffeners. However, the plate model fails to replicate the same local conditions as the beam model, particularly in the junction zones where the interaction between these components is lost. To address this issue, a two-phase calibration approach has been adopted.

In the first phase, the focus is on the flanges. To simplify the calibration process and avoid the complexity arising from the interaction between the stiffeners and flanges, substitute springs for the flanges are calibrated without considering the presence of the stiffeners. Instead, ideal constraints are applied to simulate their effects. This approach significantly reduces the number of variables involved.

Moving on to the second phase, the emphasis shifts to the stiffeners. Here, the correlations between the geometry of the flanges and the level of constraint they provide are considered. Substitute vertical springs for the stiffeners are calibrated, considering the presence of the flanges. This phase introduces a dual variability of parameters, as the effects of the same stiffener can vary depending on the dimensions of the flanges. Therefore, relationships are studied to incorporate the variability of the constraint provided by the stiffeners with changes in their dimensions and the varying flange sizes.

In the first phase, a partial model consisting of the web and flanges is developed, following the approaches of Graciano and Edlund [2], Ren and Tong [17], and Granath and Lagerqvist [27]. The constraints are applied to the vertical sides and ends of the two flanges, allowing displacements in the Δx direction and preventing displacements in the Δy and Δz directions and rotations Rx.

The 3d model is discretized using plate elements based on the geometries above. Once the first eigenvalue (λ_1) of the linear stability problem is obtained, the elastic critical load

(F_{cr}) is calculated. From this, the value of the buckling coefficient (k_{cr}) is determined using the equations:

$$F_{cr} = \lambda_1 \cdot n_{KR} \cdot F_0 = k_{cr} \cdot \frac{\pi^2 \cdot E \cdot t^3}{12 \cdot (1 - \nu^2) \cdot h}, \tag{3}$$

$$k_{cr} = \frac{(\lambda_1 \cdot n_{KR} \cdot F_0) \cdot 12 \cdot (1 - \nu^2) \cdot h}{\pi^2 \cdot E \cdot t^3}. \tag{4}$$

Here, F_0 represents the vertical load.

Referring to the six degrees of freedom (DOF) at the web-flange intersection nodes, it is considered that the stabilizing contribution of the flange can be decomposed into six overall stiffness components: three translational and three rotational. The collaboration the flanges provide can be reduced by decoupling one or more DOF of the implemented master–slave elements.

The resulting buckling coefficient of the 3d model is considered a reference term to quantify the residual contribution offered by the flanges after decoupling various DOF. By comparing this with the coefficient of the 3d model ($k_{cr,\,3d}$), an understanding can be obtained regarding the most significant stiffness contributions.

Accordingly, the main results of this paper are two:

(1) Estimating the buckling coefficient by progressively releasing the constraints of the 2d model to isolate the degree of freedom most affecting the buckling analyses;
(2) Calibrating the equivalent 2d models based on the results of the previous steps by proposing empirical regression equations as a function of adimensional parameters.

The first phase results in the following steps:

(1) The *Rz* rotations are independent: at this point, the constrained DOF are the three displacements Δx, Δy, and Δz, and the two rotations *Rx* and *Ry*.
(2) The *Ry* rotation is released: the constrained DOF are now the three displacements and the rotation *Rx*.
(3) The Δy displacements are independent: the master–slave elements still ensure the same displacements in the *x* and *z* directions and the rotation *Rx*.
(4) The *Rx* displacements are decoupled: only the Δz displacements and the rotation *Rx* remain coupled.
(5) The *Rx* rotation is released: the two flanges collaborate only in flexural behavior out of the plane.
(6) The two flanges are entirely decoupled from the web: all DOF are released.

A linear buckling analysis is conducted at each step, resulting in an eigenvalue $\lambda_{1,\,i}$, a critical load $F_{cr,\,i}$, and a buckling coefficient $k_{cr,\,i}$, where *i* denotes the step number. Significant deviations of the buckling coefficient from the original value indicate significant stiffness contributions.

An equivalent 2d model with spring elements is developed in the second phase. The objective is to replace the flanges with elastic constraints. Axial and rotational springs are implemented in the *x* direction along the horizontal sides of the model. However, considering the high-flexural inertia of the flanges in the *z* direction, a simplification is made by using fixed constraints (Δz) on the intersection nodes instead of employing high-stiffness springs.

The optimization problem, aiming to determine the optimal stiffness value ($\widehat{K}_{2d}$) for the 2d model that minimizes the difference between the predicted buckling coefficients of the 3d and 2d models, was solved using the least squares method. The objective function was formulated as the absolute difference between the buckling coefficient predicted by the 3d model ($k_{cr,\,3d}$) and the buckling coefficient obtained from the 2d model ($k_{cr,\,2d}$), as expressed by Equation (5) as follows:

$$f(K_{2d}) = \left| k_{cr,3d} - k_{cr,2d}(K_{2d}) \right|, \tag{5}$$

where $k_{cr,\,2d}$ is the buckling coefficient predicted by the 2d model with the stiffness value K_{2d}. By applying the least squares method, the stiffness value of the 2d model was adjusted iteratively to minimize the sum of squared differences between the predicted and actual buckling coefficients, as shown in Equation (6).

$$\widehat{K}_{2d} = \min_{K_{2d}} \sum \left(k_{cr,3d} - k_{cr,2d}(K_{2d}) \right)^2. \tag{6}$$

The resulting optimal stiffness value ($\widehat{K}_{2d}$) represents the best fit between the 2d and 3d models regarding buckling behavior.

Specifically, elastic constants $K_{Rx,\,u}$ and $K_{Tx,\,u}$ are introduced and adjusted based on the buckling coefficient obtained from the previous phase to calibrate the rotational and translational springs, respectively. The same procedure is repeated for the lower flange, resulting in $K_{Rx,\,l}$ and $K_{Tx,\,l}$ values. The upper and lower edges add translational springs in the *x* direction. The stiffness values $K_{Tx,\,u}$ and $K_{Tx,\,u}$ are determined to obtain the eigenvalues of the original problem. Furthermore, the two horizontal sides are constrained in the *z* direction.

The numerical values of the elastic constants for the implemented springs, assigned to the perimeter nodes, have the following dimensional quantities: translational springs are measured in F/L. In contrast, rotational springs have dimensions of $F{\cdot}L/\theta$.

Focusing on the rotational springs in the *x* direction, their contribution replaces the effect of the flange's torsional stiffness. This effect is influenced by the dimensions of the flange (t_f and b_f) and the dimensions of the web (t and h). A common practice is to assess the flange's torsional effect relative to the plate's flexural stiffness using the dimensionless parameter $\beta = \frac{b_f \cdot t_f^3}{h \cdot t^3}$.

In addition to solving the optimization problem using the least squares method, regression equations were derived to establish relationships between the optimal stiffness value

Table 1: Parameter values.

Parameter	Values
h (Web height)	1000 mm
a (Panel length)	1,000, 2,000, and 3,000 mm
t (Web thickness)	4 mm, 8 mm, 12 mm
t_f (Flange thickness)	$1.5t$, $2t$, $2.5t$
b_f (Flange width)	$8t_f$, $10t_f$, $12t_f$
s_s (Load application length)	$0.2a$, $0.5a$, a

($\widehat{K}_{2d}$) and the adimensional parameters, namely β, β', and γ. These parameters, defined in the initial list of symbols and notation, provide insights into the geometric characteristics of the structure and the degree of constraint the flanges and stiffeners provide.

Through statistical analysis and curve fitting techniques, regression equations of the form $K_{2d} = f(\beta, \beta', \gamma)$ were developed to capture the dependence of the optimal stiffness on these adimensional parameters. These equations allow for the estimation of the optimal stiffness value based on the specific geometric configuration of the structure.

Overall, the optimization process, combined with the regression analysis, enables the calibration of the 2d model and establishes empirical relationships that facilitate the selection of the optimal stiffness value based on the geometric parameters of the structure.

2.3. Parametric Analyses. A reference model based on a symmetrical double T-shaped beam with flanges is initially modeled, following the approach outlined in [2, 17, 27, 28]. Subsequently, symmetrical stiffeners are added perpendicular to the web plane, enhancing the model's representation. Table 1 shows the parameters assumed constant and varied in the analyses.

Three different ratios ($a/h = 1$, 2, and 3) are examined to assess the influence of the subpanel aspect ratio. The external load is applied as vertical nodal forces on the upper flange, with three load configurations ($s_s/a = 0.2$, 0.5, and 1) covering a wide range from localized to uniform load. The load is applied at the web plane level, allowing separate flanges and web modeling. Through master–slave connections, the contribution of the flanges' constraints in buckling is isolated and replicated using elastic constraints. This approach prevents additional stabilizing effects that could occur if the load were applied to the extrados of the upper flange, where the load might disperse over a larger portion of the web. The web and flanges are assigned different plate properties for the parametric investigation while maintaining their mechanical characteristics. Following the guidelines by Ren and Tong [17], a uniform reference size is established with a web height (h) of 1,000 mm. Geometric dimensions are derived accordingly, with panel lengths (a) of 1,000, 2,000, and 3,000 mm, and the web thickness adjusted to achieve three different panel slenderness values (λ).

Consistent with [17], the web thickness (t) is set to 4, 8, and 12 mm, corresponding to 250, 125, and 83 slenderness values. Flange thickness (t_f) is defined as 1.5 t, 2 t, and 2.5 t, and the flange width (b_f) is determined using standard ratios, specifically semiwidths of 8 t_f, 10 t_f, and 12 t_f. To cover the desired load configurations, load application lengths (s_s) are assumed relative to the panel length: $s_s = 0.2\,a$, $0.5\,a$, and a. Square elements with a side length of 25 mm (h/40) are chosen for the web, while elements with a length of 25 mm in the x-direction are used for the flanges, with varying lengths in the y-direction based on the total width. This approach ensures that the web, most affected by buckling, is appropriately modeled.

In conclusion, 324 cases are examined to cover the flanges' full range of patch load variability. This involves considering three aspect ratios ($a/h = 1$, 2, and 3) and three load configurations ($s_s/a = 0.2$, 0.5, and 1). Each case includes variations in web thickness, flange width, and flange thickness, resulting in nine configurations for each combination. Panel lengths (a) are set to 1,000, 2,000, and 3,000 mm, determining slenderness values of 250, 125, and 83. Flange thickness (t_1) is chosen as t, 1.5 t, 2 t, and 2.5 t, while flange width (b_1) is defined as 8, 10, and 12 t_1.

3. FE Model Validation

To ensure the accuracy and reliability of the proposed methodology, both the 2d and 3d models were assessed through calibration and validation processes. The 2d model was calibrated to ensure consistent and accurate results by adjusting the spring constants to match the buckling coefficients obtained from the comprehensive 3d model. On the other hand, the 3d model was validated to assess its ability to accurately predict the system's buckling behavior. The validation process involved comparing the results obtained from the 3d model, utilizing Quad4 and Quad8 plate elements, to verify their consistency. Quad4 and Quad8 are FE types commonly used for modeling plate structures in FE analysis.

(i) Quad4: Quad4 refers to a quadrilateral element with four nodes. It is also known as a bilinear quadrilateral element. In this element, each node has two DOFs, typically representing displacements in the x and y directions. The nodal coordinates define the element and can accurately capture linear variations in displacement and stress within the element.

(ii) Quad8: Quad8 refers to a quadrilateral element with eight nodes. It is also known as a quadratic quadrilateral element. Similar to Quad4, each node of Quad8 has two DOFs. Quad8 provides additional nodes compared to Quad4, allowing for higher order interpolation and a more accurate representation of curved or nonlinear variations in displacement and stress within the element. This element type can capture higher order deformations more effectively.

Due to their simplicity and versatility, Quad4 and Quad8 elements are widely used in the structural analysis, including plate and shell modeling. The choice between Quad4 and Quad8 depends on the desired level of accuracy and computational efficiency for a specific analysis.

The difference in the resulting buckling coefficients between the two cases was less than 1%, indicating a high

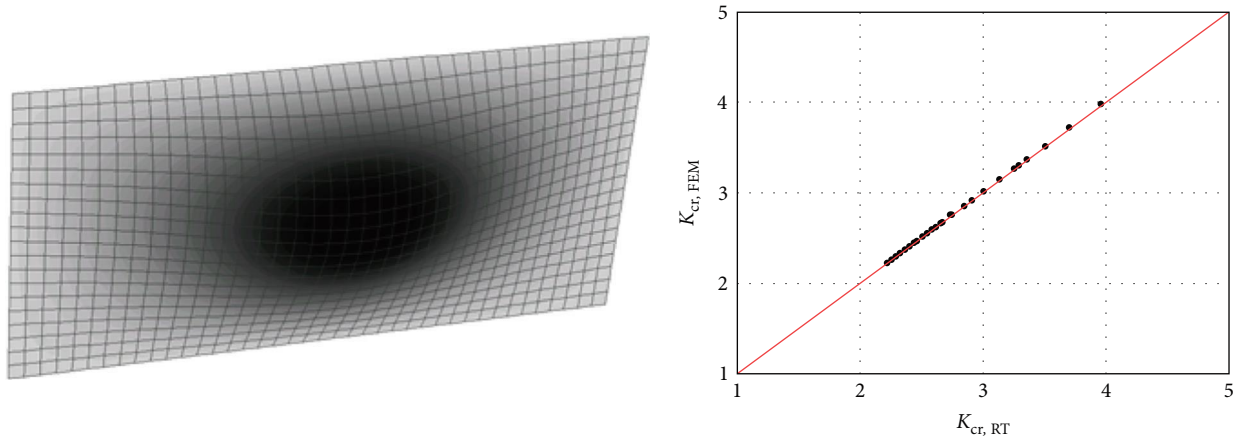

(a) (b)

FIGURE 3: (a) Typical buckled configuration; (b) comparison between $k_{cr,\,FEM}$ and $k_{cr,\,RT}$ [17] for the finite-rigidity restrained 2d model.

level of agreement. Additionally, nodal forces were applied to maintain a constant load direction during the buckling analysis to maintain realistic boundary conditions. The models' sides were hinged, as illustrated in Figure 3.

To assess the impact of mesh refinement, two additional models were created using Quad4 plate elements. One model had a finer mesh, while the other had a coarser mesh. By increasing or decreasing the number of elements by a factor of four, the coarser mesh allowed for a more explicit identification of differences than the original model. The coarser mesh resulted in a higher critical load, and as the mesh refinement increased, the buckling coefficient (k_{cr}) approached a constant value.

To validate the model, a comparison was conducted with the results reported in Ren and Tong [17] for a finite-rigidity restrained 2d model, considering various patch load lengths ranging from 0.05 to 3. The comparison revealed a close agreement between the calculated values and those reported in Ren and Tong [17], indicating the model's accuracy. The obtained results showed a very low error, with discrepancies within the range of 1% to 2% (Figure 3(b)).

Equation (7), proposed by Graciano and Lagerqvist [3], was referenced for the subsequent analysis. This equation allows for the evaluation of the buckling coefficient (k_{cr}) of a rectangular plate subjected to a concentrated force applied through the upper flange and balanced by shear forces in the web:

$$k_{cr} = 5.82 + 2.1\left(\frac{h}{a}\right)^2 + 0.46\beta^{1/4}. \quad (7)$$

As anticipated, $\beta = \frac{b_1 t_1^3}{ht^3}$ represents a parameter that quantifies the rotational constraint provided by the flanges. As β approaches 0, the plate is hinged at the edges, while approaching infinity indicates clamping. In real cases, the degree of constraint lies between these two extremes, resulting in a wide range of critical loads based on the geometric dimensions of the flanges and web panels. The results obtained from the numerical calculations using the model with incorporated flanges (Figure 4) were compared to those reported in [3]. The comparison depicted in Figure 5(a) revealed a significant agreement between the values obtained, confirming the model's accuracy.

Furthermore, Graciano and Lagerqvist [2] studied the elastic critical load by varying the lengths of application of localized loads. The numerical results obtained for load lengths of 0, 0.1, 0.25, 0.3, 0.4, and 0.5 were compared to the findings in [3]. The comparison, presented in Figure 5(b), demonstrated a good coincidence between the values, further supporting the model's validity.

4. Results

The results obtained from the analysis play a crucial role in validating and fine-tuning the FE model developed in this study. This section presents a detailed examination of the calibration process for the equivalent spring representing the flanges and the behavior of the stiffeners. The first subsection focuses on calibrating the equivalent spring, aiming to accurately capture the response of the flanges under various loading conditions. The subsequent subsection delves into the behavior of the stiffeners within the structural system. Stiffeners are critical components that enhance the overall strength and stability of the plate structure. The results provide a solid foundation for further discussions and conclusions regarding the structural response and performance of the plate structure under the different loading scenarios.

4.1. Equivalent 2d Model for the Flanges. Table 2 presents the buckling coefficients obtained at each step of the progressive constraint release of the plate, as described in the methodology section. The table provides a comprehensive overview of the results, showcasing the calculated buckling coefficients for different geometric configurations and load scenarios. The buckling coefficients (k_{cr}) are reported for various combinations of parameters, including the aspect ratio (a), web height (h), web thickness (t), flange thickness (t_1), flange width (b_1), and the defect levels (a, b, c, d, e, f, g, h, and i).

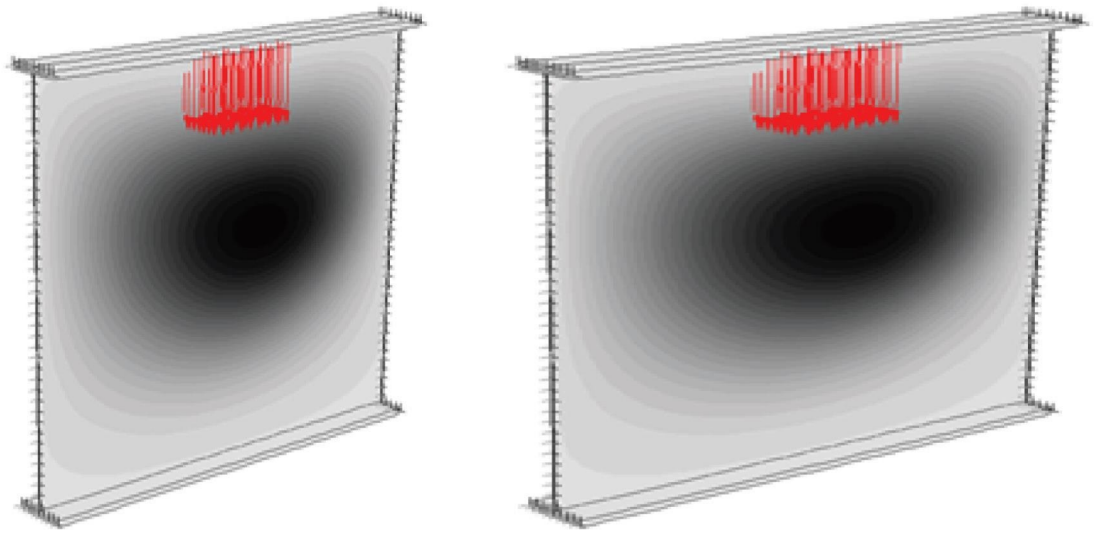

(a) (b)

FIGURE 4: Buckled configuration for panels with (a) $a/s_s = 1$, $t = 4$ mm, $t_1 = 16$ mm, and $b_1 = 125$ mm and (b) $a/s_s = 2$, $t = 4$ mm, $t_1 = 16$ mm, and $b_1 = 250$ mm.

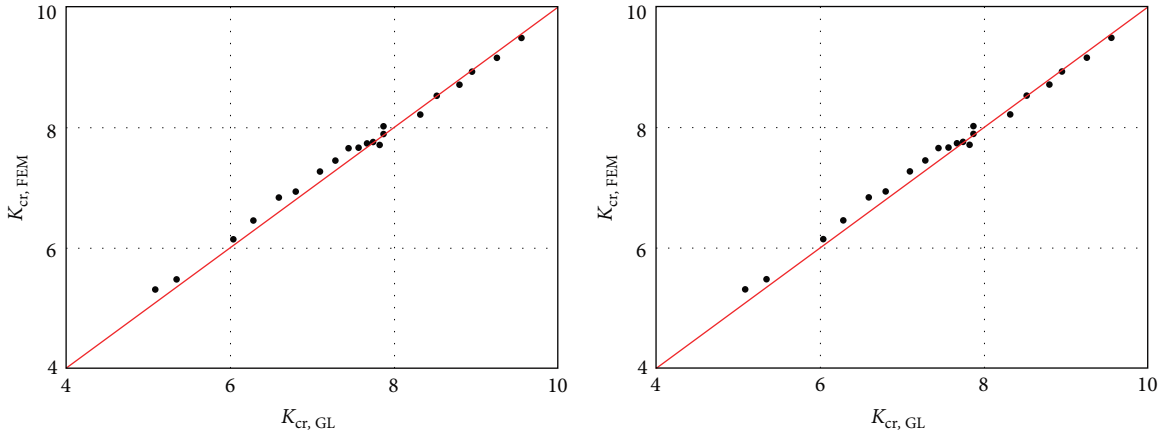

(a) (b)

FIGURE 5: (a) Comparison between $k_{cr, FEM}$ and $k_{cr, GL}$ for $b_1 = 125$ mm and 250 mm; (b) comparison between $k_{cr, FEM}$ and $k_{r, GL}$ [2] for the model with varying load length.

TABLE 2: Buckling coefficients for each step of the progressive constraint realizing of the plate, as explained in the methodology section.

n	s_s/a	a	h	t	t_1	b_1	$k_{cr, 3d}$	$k_{cr, 1}$	$k_{cr, 2}$	$k_{cr, 3}$	$k_{cr, 4}$	$k_{cr, 5}$	$k_{cr, 6}$
a	0.2	1,000	1,000	12	30	480	8.209	8.209	8.209	8.106	6.821	3.344	0.934
b	0.2	2,000	1,000	4	6	120	3.488	3.488	3.488	3.488	3.247	2.524	0.347
c	0.2	3,000	1,000	4	8	160	4.269	4.269	4.269	4.269	3.846	2.536	0.174
d	0.5	1,000	1,000	8	16	256	8.576	8.576	8.576	8.567	7.328	3.959	1.13
e	0.5	2,000	1,000	8	12	240	5.085	5.085	5.085	5.084	4.743	3.177	0.406
f	0.5	3,000	1,000	8	10	400	8.941	8.941	8.941	8.939	8.095	3.633	0.2
g	1	1,000	1,000	4	10	240	13.79	13.79	13.791	13.79	11.79	6.221	1.762
h	1	2,000	1,000	12	18	360	9.025	9.025	9.025	9.026	8.513	5.13	0.615
i	1	3,000	1,000	12	24	576	13.81	13.81	13.812	13.81	12.97	6.171	0.3

Specifically, the behavior of the three models was analyzed for each load configuration of 0.2, 0.5, and 1, considering the aspect ratios of 1, 2, and 3. The dimensions of the models are shown in Table 2, and the corresponding buckling coefficients (k_{cr}) at each step of the analysis are directly listed.

The table reveals that the progressive constraint release in the 2d model leads to a gradual decrease in the buckling coefficients as the model evolves through each step. The largest discrepancies between the buckling coefficients obtained from the 3d model ($k_{cr,3d}$) and the corresponding steps in the 2d model ($k_{cr,1}$ to $k_{cr,6}$) are observed in steps $i = 3$ and $i = 4$. Decoupling specific DOF in the 2d model has varying effects on the critical load and buckling coefficient. For example, decoupling the Ry and Rz rotations ($i = 1, 2$) does not affect the eigenvalue. However, decoupling the vertical displacements of the intersection nodes ($i = 3$) slightly modifies the critical load. Decoupling the Δz displacements ($i = 4$) significantly impacts the critical load and the buckling coefficient. Furthermore, decoupling the Rx and Dz DOFs at step $i = 6$ allows the web to rotate and move out of its plane, substantially affecting the critical load.

These discrepancies in the buckling coefficients highlight the significance of the calibration process and the progressive inclusion of constraints in the 2d model. They demonstrate the importance of accurately capturing the interaction between different components of the plate and the influence it has on the overall buckling behavior. In conclusion, the significant stiffness provided by the two flanges is related to the degrees of freedom Δx, Δy, and Rx. Replacing the flanges with elastic constraints involved setting axial and rotational springs in the x direction. However, it was found that it is better to assign a fixed constraint $\Delta z = 0$ rather than using high elastic constants for the springs, considering the high flexural inertia of the flanges in the z direction.

To investigate the rotational effect of the flange in comparison to the bending stiffness of the plate, the dimensionless parameter β was used. The relative rotational stiffness, denoted as $k_{R,rel}$, can be calculated using Equation (8), where K_R represents the rotational stiffness per unit length.

$$k_{R,rel} = 12 \cdot K_R \cdot n_{kr} \cdot (1 - \nu^2) \frac{h}{E \cdot t^3 \cdot a}. \tag{8}$$

Similarly, the translational effect of the flange was examined concerning the axial stiffness of the plate using the dimensionless parameter $\gamma = \frac{b_1 \cdot t_1}{h \cdot t}$. The relative translational stiffness, denoted as $k_{T,rel}$, is determined by Equation (9), with K_T representing the axial stiffness per unit length.

$$k_{T,rel} = 12 \cdot K_T \cdot n_K \frac{h}{E \cdot t \cdot a}. \tag{9}$$

In the analysis, a fixed constraint was applied in the z direction to restrict any out-of-plane movement. To ensure an equal number of nodes on the two horizontal sides (n_k), the element sizes were scaled to match the magnitude of h, considering three scaling factors (0.5, 0.25, and 1.5).

Table 3: Determination of $K_{R,rel}$ for upper and lower flanges.

a/h	s_s/a	Upper flange	Lower flange
1	0.2	$K_{R,rel} = 14.2890\,\beta$	$K_{R,rel} = 13.1840\,\beta$
1	0.5	$K_{R,rel} = 13.5510\,\beta$	$K_{R,rel} = 13.2590\,\beta$
1	1	$K_{R,rel} = 14.81200\,\beta$	$K_{R,rel} = 14.0620\,\beta$
2	0.2	$K_{R,rel} = 14.3450\,\beta$	$K_{R,rel} = 4.5440\,\beta$
2	0.5	$K_{R,rel} = 14.2880\,\beta$	$K_{R,rel} = 4.2160\,\beta$
2	1	$K_{R,rel} = 14.4850\,\beta$	$K_{R,rel} = 4.0810\,\beta$
3	0.2	$K_{R,rel} = 14.7551\,\beta$	$K_{R,rel} = 3.4313\,\beta$
3	0.5	$K_{R,rel} = 14.4703\,\beta$	$K_{R,rel} = 2.7307\,\beta$
3	1	$K_{R,rel} = 14.6496\,\beta$	$K_{R,rel} = 1.9030\,\beta$

Table 3 and Figure 6 present the correlation results between the rotational springs $k_{R,rel}$ and the dimensionless parameter β for the upper and lower flanges. The table demonstrates the strong relationship between these variables, as indicated by the high quality of the regression models with R^2 higher than 0.95.

A comprehensive analysis of the obtained numerical values reveals the following key observations:

(i) With the panels transition from square to elongated shapes, there is a consistent decrease in $K_{R,rel}$ while maintaining a constant load condition and β parameter. This trend is captured accurately by the regression models.

(ii) The relative rotational stiffness ($K_{R,rel}$) is found to be more sensitive to the parameter γ (flange width-to-web thickness ratio) than the specific loading configuration. The regressions exhibit excellent performance in capturing this sensitivity.

(iii) For aspect ratios of 2 and 3, the rotational stiffness around the upper flange decreases with increasing γ. In contrast, the rotational stiffness around the lower flange decreases from 0.2 to 0.5 and then increases between 0.5 and 1. The regressions accurately represent these variations.

(iv) The behavior of the square panel differs from that of the two rectangular panels. For an aspect ratio of 1, with load configurations of 0.2 and 0.5, the relative stiffness of the upper flange is greater than that of the lower flange. However, this trend is reversed when transitioning to an aspect ratio 1. The regression models successfully capture these trends.

The quality of the regression models can be assessed by various metrics, including the coefficient of determination (R^2). The R^2 values exceed 0.95 in all cases, indicating a strong correlation between the rotational springs ($k_{R,rel}$) and the dimensionless parameter β. The excellent R^2 values suggest that the regressions provide accurate and reliable estimates of the rotational stiffness based on the geometric parameters.

These findings highlight the robustness and reliability of the regression models in capturing the relationship between the rotational stiffness and the adimensional parameters,

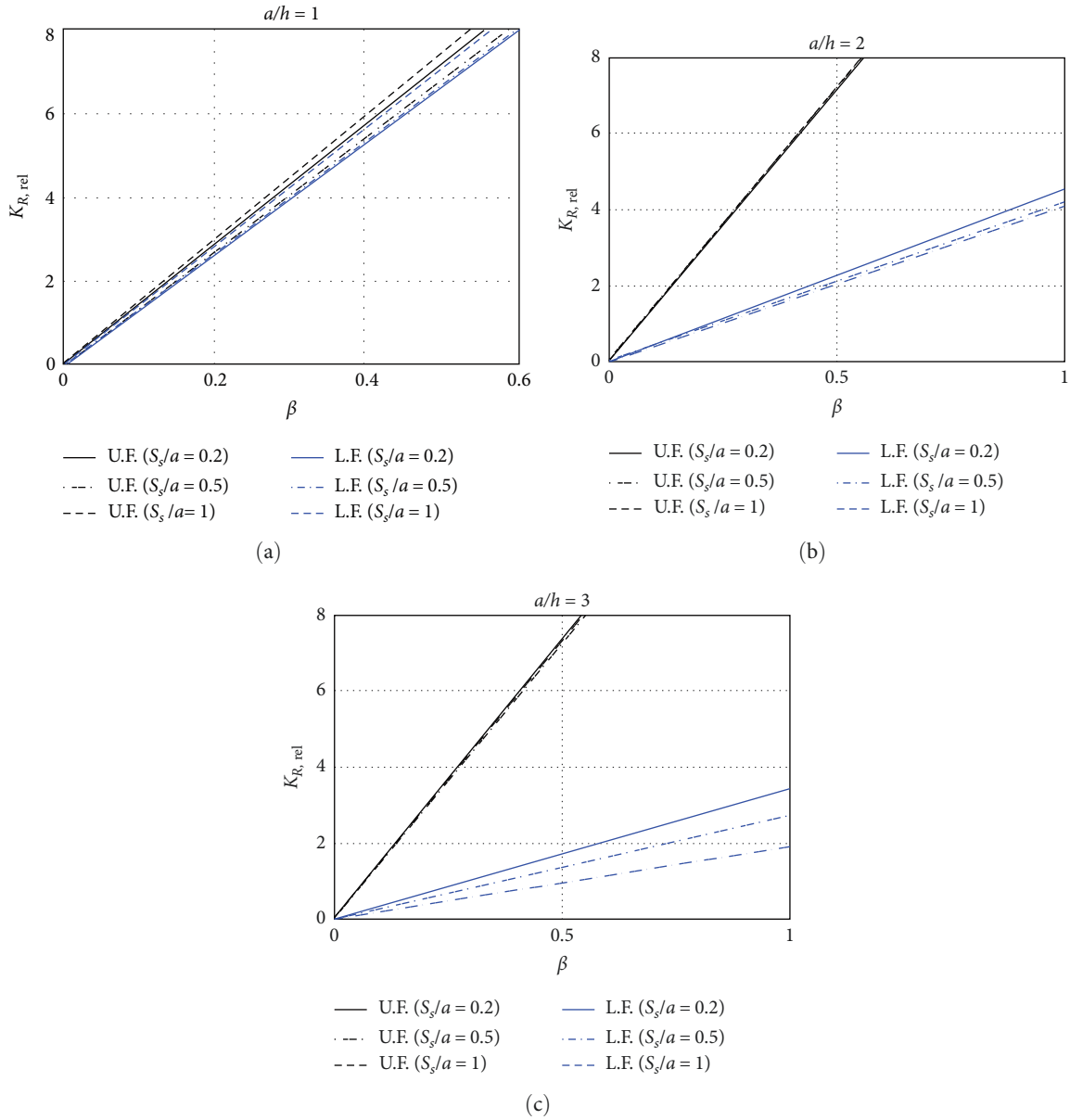

FIGURE 6: Plots of $k_{R,\text{rel}}$ against β for different values of s_s/a and a/h. The three subfigures represent the different upper (U.F.) and lower flanges (L.F.) scenarios given $a/h = 1, 2$ and 3, respectively.

providing valuable insights into the system's behavior under different geometric configurations and load conditions.

Table 4 and Figure 7 presents the relationship between the translational springs $K_{T,\text{rel}}$ and the dimensionless parameter γ for the upper and lower flanges. The table provides valuable insights into the relationship between these variables, shedding light on the system's behavior under different geometric configurations and load conditions.

A comprehensive analysis of the numerical values reveals the following key observations:

(i) Varying the aspect ratio of the panels results in different behaviors regarding the translational stiffness. As the panels' shape changes from a square to elongated, there is a consistent decrease in $K_{T,\text{rel}}$ while maintaining a constant load condition and γ parameter. This trend, captured by the regression models, demonstrates the sensitivity of the translational stiffness to the aspect ratio.

(ii) The relative translational stiffnesses ($K_{T,\text{rel}}$) are found to be more sensitive to the parameter γ (flange width-to-web thickness ratio) than to the specific loading configuration. The regressions accurately capture this sensitivity, highlighting the importance of the ratio γ in determining the translational behavior of the flanges.

(iii) When the load is distributed over the length a, the translational contribution of the two flanges becomes more uniform. This indicates that a more distributed load leads to a more balanced sharing of

Table 4: Determination of $K_{T,\mathrm{rel}}$ for upper and lower flanges.

a/h	s_s/a	Upper flange	Lower flange
1	0.2	$K_{T,\mathrm{rel}} = 0.489\,\gamma^3 - 4.279\,\gamma^2 + 11.372\,\gamma$	$K_{T,\mathrm{rel}} = 0.310\gamma^3 - 3.411\,\gamma^2 + 9.870\,\gamma$
	0.5	$K_{T,\mathrm{rel}} = 0.364\,\gamma^3 - 3.710\,\gamma^2 + 10.438\,\gamma$	$K_{T,\mathrm{rel}} = 0.314\gamma^3 - 3.421\,\gamma^2 + 9.873\,\gamma$
	1	$K_{T,\mathrm{rel}} = 0.253\,\gamma^3 - 3.103\gamma^2 + 9.288\,\gamma$	$K_{T,\mathrm{rel}} = 0.302\gamma^3 - 3.391\,\gamma^2 + 9.854\,\gamma$
2	0.2	$K_{T,\mathrm{rel}} = -0.440\,\gamma^2 + 3.364\,\gamma$	$K_{T,\mathrm{rel}} = -0.348\,\gamma^2 + 2.627\,\gamma$
	0.5	$K_{T,\mathrm{rel}} = -0.345\,\gamma^2 + 2.722\,\gamma$	$K_{T,\mathrm{rel}} = -0.338\,\gamma^2 + 2.558\,\gamma$
	1	$K_{T,\mathrm{rel}} = -0.325\,\gamma^2 + 2.399\,\gamma$	$K_{T,\mathrm{rel}} = -0.331\,\gamma^2 + 2.502\,\gamma$
3	0.2	$K_{T,\mathrm{rel}} = 1.551\,\gamma$	$K_{T,\mathrm{rel}} = 1.204\,\gamma$
	0.5	$K_{T,\mathrm{rel}} = 1.142\,\gamma$	$K_{T,\mathrm{rel}} = 1.082\,\gamma$
	1	$K_{T,\mathrm{rel}} = 1.037\,\gamma$	$K_{T,\mathrm{rel}} = 1.033\,\gamma$

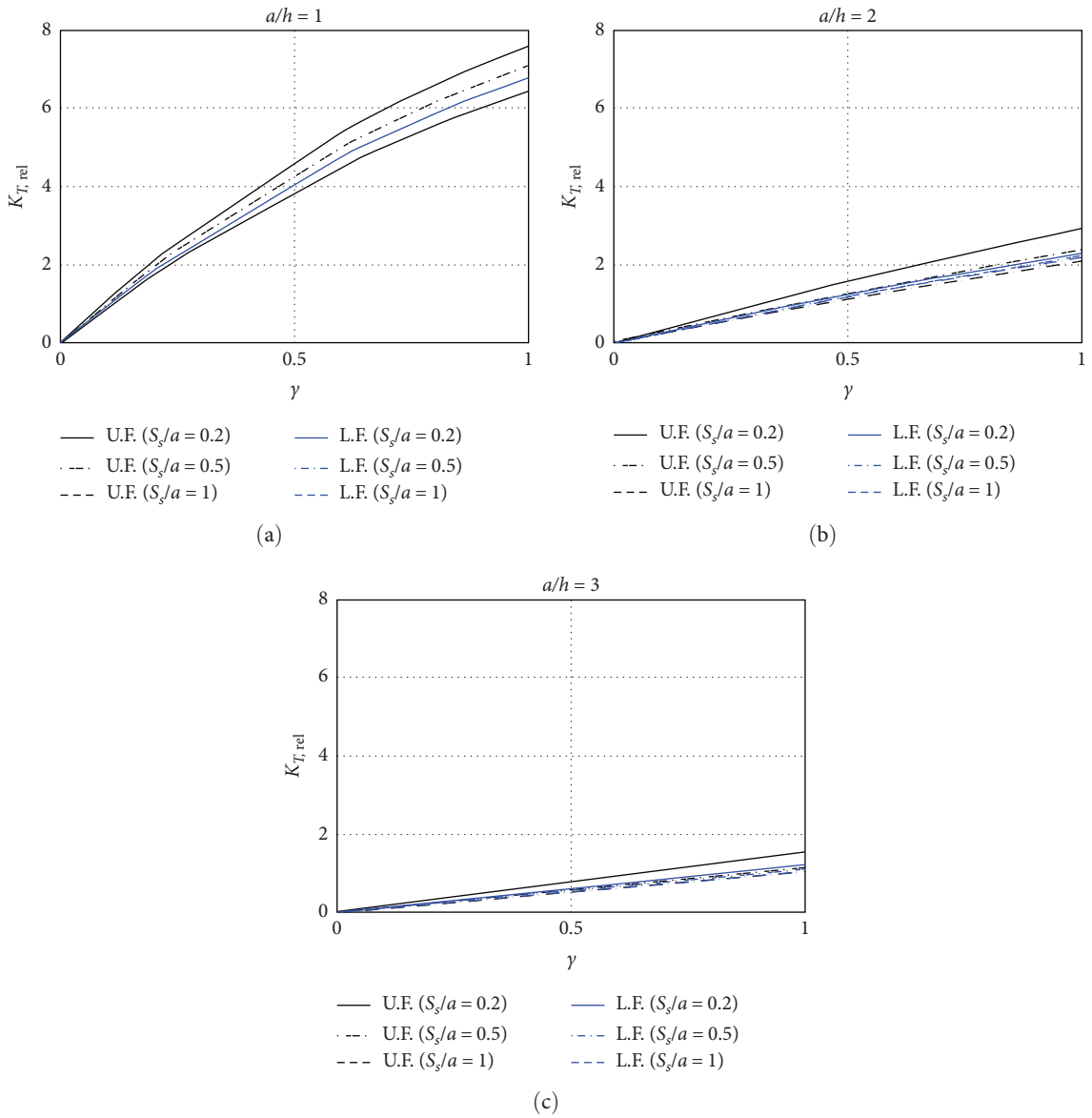

Figure 7: Plots of $k_{T,\mathrm{rel}}$ against γ for different values of s_s/a and a/h. The three subfigures represent the different upper (U.F.) and lower flanges (L.F.) scenarios given $a/h = 1, 2$ and 3, respectively.

Table 5: Buckling coefficients of the 2d model for each step-wise constraint releasing method phase.

No.	s_s/a	a	h	t	t_1	b_1	t_2	b_2	$k_{cr,3d}$	$k_{cr,1}$	$k_{cr,2}$	$k_{cr,3}$	$k_{cr,4}$	$k_{cr,5}$	$k_{cr,6}$
a	0.2	1,000	1,000	12	24	480	12	144	8.685	8.685	8.685	8.684	8.684	7.915	6.218
b	0.2	2,000	1,000	4	8	160	6	48	4.74	4.74	4.74	4.74	4.74	4.681	4.652
c	0.2	3,000	1,000	8	12	240	12	96	3.873	3.873	3.873	3.873	3.873	3.853	3.845
d	0.5	1,000	1,000	8	16	320	8	96	9.573	9.573	9.573	9.573	9.573	8.807	6.427
e	0.5	2,000	1,000	12	12	240	18	114	4.194	4.194	4.194	4.194	4.194	3.953	3.829
f	0.5	3,000	1,000	4	6	72	10	200	7.485	7.485	7.485	7.485	7.485	7.465	7.444
g	1	1,000	1,000	4	6	120	6	58	11.437	11.44	11.44	11.44	11.44	9.712	6.16
h	1	2,000	1,000	8	20	400	12	96	13.68	13.68	13.68	13.68	13.68	13.23	12.18
i	1	3,000	1,000	12	18	360	18	144	9.623	9.623	9.623	9.624	9.623	9.389	9.146

the translational stiffness between the upper and lower flanges. The regressions effectively represent this relationship.

(iv) For each observed geometric configuration with load configurations of 0.2 and 0.5, it is observed that the relative stiffness of the upper flange is generally more significant than that of the lower flange. However, this trend may be reversed when transitioning to an aspect ratio 1. The regression models accurately capture these variations, providing valuable insights into the relative stiffnesses of the flanges.

(v) For aspect ratios 2 and 3, the relative translational stiffness of the flanges decreases with increasing γ, indicating a stronger contribution of the flanges to the overall stiffness. Interestingly, when aspect ratio 3 is compared with aspect ratio 1, both flanges exhibit similar values of the relative translational stiffness. This observation emphasizes the importance of considering the geometric configuration in understanding the translational behavior of the flanges.

These findings provide valuable insights into the relationship between the translational springs and the adimensional parameter γ. The high quality of the regression models is evident in their ability to accurately capture the behavior of the translational stiffness of the geometric parameters. Overall, the results demonstrate the effectiveness of the regressions in characterizing the translational behavior of the flanges and their contribution to the overall system stiffness.

4.2. Equivalent 2d Model for the Transverse Stiffening. Table 5 displays the buckling coefficients (k_{cr}) for each stage of analysis, represented by $k_{cr,i}$, where i goes from 1 to 6. These stages correspond to the systematic release of constraints across six phases previously outlined. The table provides insights into how the 2d model responds to the step-by-step relaxation of constraints. Both geometric changes and steel defect levels influence the buckling coefficients. For reference, the buckling coefficients for the 3d model ($k_{cr,3d}$) are included, while coefficients $k_{cr,1}$ to $k_{cr,6}$ detail the results for each of the six phases.

Analyzing the numerical values, several noteworthy observations can be made:

(i) The most significant variations in buckling coefficients are observed in square panels. As the aspect ratio (a/h) increases, the panels become less sensitive to the characteristics of the stiffeners. This indicates that the stiffeners' influence on the panel's buckling behavior decreases as the aspect ratio increases.

(ii) Additionally, the data in the table suggests that the most considerable reductions in buckling coefficients occur for higher aspect ratio values. This implies that higher aspect ratio panels exhibit a more significant reduction in their sensitivity to the lateral boundary conditions imposed by the stiffeners.

These findings highlight the influence of the aspect ratio and the stiffeners' characteristics on the panels' buckling behavior. The observed variations in buckling coefficients provide insights into the sensitivity of the panels to different geometric and boundary conditions. As the aspect ratio increases and the influence of the stiffeners decreases, the panels exhibit reduced sensitivity to lateral boundary conditions. In conclusion, the results from Table 5 demonstrate that the sensitivity of the panels to the lateral boundary conditions increases with a decrease in aspect ratio and a corresponding increase in the influence of the stiffeners. These findings contribute to a better understanding of the relationship between geometric parameters, boundary conditions, and the buckling behavior of the panels, providing valuable insights for the design and analysis of similar structures.

Rotational springs around the y-axis were introduced to incorporate the stiffness of the stiffeners. The rotational stiffness is influenced by the dimensions of the stiffening elements, specifically t_2 and b_2, as well as the size of the web panel represented by t and a. To evaluate the rotational rigidity of the plate stiffness, a term denoted as the relative rotational stiffness, $K_{R,rel}$, was introduced. The relationship between β' and $K_{R,rel}$ in the z-direction, where out-of-plane movements were eliminated, is established and presented in Table 6.

Table 6 provides the determination of $K_{R,rel}$ for the stiffeners, presenting the variation in relative rotational stiffness

Table 6: Determination of $K_{R,\mathrm{rel}}$ regressions for stiffeners.

a/h	s_s/a	λ	β	$K_{R,\mathrm{rel}}$	a/h	s_s/a	λ	β	$K_{R,\mathrm{rel}}$
	0.2	83.3	>0.08	$K_{R,\mathrm{rel}} = 21.462\ \beta'$	3	0.2	250	0.08	$K_{R,\mathrm{rel}} = 340.560\ \beta'$
1	0.5	250	<9.38	$K_{R,\mathrm{rel}} = 21.811\ \beta'$				0.41	$K_{R,\mathrm{rel}} = 136.300\ \beta'$
	1			$K_{R,\mathrm{rel}} = 22.383\ \beta'$				1.28	$K_{R,\mathrm{rel}} = 148.020\ \beta'$
		250	0.08	$K_{R,\mathrm{rel}} = 61.643\ \beta'$				3.13	$K_{R,\mathrm{rel}} = 187.00\ \beta'$
			0.41	$K_{R,\mathrm{rel}} = 62.265\ \beta'$	3	0.2	125	0.16	$K_{R,\mathrm{rel}} = 171.490\ \beta'$
2	0.2		1.28	$K_{R,\mathrm{rel}} = 67.674\ \beta'$				0.81	$K_{R,\mathrm{rel}} = 141.050\ \beta'$
			3.13	$K_{R,\mathrm{rel}} = 77.813\ \beta'$				2.56	$K_{R,\mathrm{rel}} = 169.520\ \beta'$
		125	0.16	$K_{R,\mathrm{rel}} = 60.955\ \beta'$				6.25	$K_{R,\mathrm{rel}} = 291.530\ \beta'$
			0.81	$K_{R,\mathrm{rel}} = 64.410\ \beta'$	3	0.2	83.3	0.24	$K_{R,\mathrm{rel}} = 136.460\ \beta'$
2	0.2		2.56	$K_{R,\mathrm{rel}} = 72.475\ \beta'$				1.22	$K_{R,\mathrm{rel}} = 141.940\ \beta'$
			6.25	$K_{R,\mathrm{rel}} = 84.964\ \beta'$				3.84	$K_{R,\mathrm{rel}} = 187.300\ \beta'$
		83.3	0.24	$K_{R,\mathrm{rel}} = 62.126\ \beta'$				9.38	$K_{R,\mathrm{rel}} = 460.380\ \beta'$
			1.22	$K_{R,\mathrm{rel}} = 65.252\ \beta'$	3	0.5	250	0.08	$K_{R,\mathrm{rel}} = 404.090\ \beta'$
2	0.2		3.84	$K_{R,\mathrm{rel}} = 73.919\ \beta'$				0.41	$K_{R,\mathrm{rel}} = 142.030\ \beta'$
			9.38	$K_{R,\mathrm{rel}} = 86.035\ \beta'$				1.28	$K_{R,\mathrm{rel}} = 156.720\ \beta'$
		250	0.08	$K_{R,\mathrm{rel}} = 62.993\ \beta'$				3.13	$K_{R,\mathrm{rel}} = 211.780\ \beta'$
			0.41	$K_{R,\mathrm{rel}} = 63.773\ \beta'$	3	0.5	125	0.16	$K_{R,\mathrm{rel}} = 175.990\ \beta'$
2	0.5		1.28	$K_{R,\mathrm{rel}} = 68.870\ \beta'$				0.81	$K_{R,\mathrm{rel}} = 145.870\ \beta'$
			3.13	$K_{R,\mathrm{rel}} = 78.280\ \beta'$				2.56	$K_{R,\mathrm{rel}} = 183.00\ \beta'$
		125	0.16	$K_{R,\mathrm{rel}} = 62.467\ \beta'$				6.25	$K_{R,\mathrm{rel}} = 375.560\ \beta'$
			0.81	$K_{R,\mathrm{rel}} = 65.672\ \beta'$	3	0.5	83.3	0.24	$K_{R,\mathrm{rel}} = 140.250\ \beta'$
2	0.5		2.56	$K_{R,\mathrm{rel}} = 73.090\ \beta'$				1.22	$K_{R,\mathrm{rel}} = 148.840\ \beta'$
			6.25	$K_{R,\mathrm{rel}} = 83.600\ \beta'$				3.84	$K_{R,\mathrm{rel}} = 214.110\ \beta'$
		83.3	0.24	$K_{R,\mathrm{rel}} = 63.577\ \beta'$				9.38	$K_{R,\mathrm{rel}} = 500.340\ \beta'$
			1.22	$K_{R,\mathrm{rel}} = 66.308\ \beta'$	3	1	250	0.08	$K_{R,\mathrm{rel}} = 313.880\ \beta'$
2	0.5		3.84	$K_{R,\mathrm{rel}} = 73.898\ \beta'$				0.41	$K_{R,\mathrm{rel}} = 153.360\ \beta'$
			9.38	$K_{R,\mathrm{rel}} = 83.289\ \beta'$				1.28	$K_{R,\mathrm{rel}} = 171.400\ \beta'$
		250	0.08	$K_{R,\mathrm{rel}} = 65.707\ \beta'$				3.13	$K_{R,\mathrm{rel}} = 221.810\ \beta'$
			0.41	$K_{R,\mathrm{rel}} = 67.284\ \beta'$	3	1	125	0.16	$K_{R,\mathrm{rel}} = 168.700\ \beta'$
2	1		1.28	$K_{R,\mathrm{rel}} = 72.916\ \beta'$				0.81	$K_{R,\mathrm{rel}} = 158.200\ \beta'$
			3.13	$K_{R,\mathrm{rel}} = 82.345\ \beta'$				2.56	$K_{R,\mathrm{rel}} = 196.000\ \beta'$
		125	0.16	$K_{R,\mathrm{rel}} = 65.519\ \beta'$				6.25	$K_{R,\mathrm{rel}} = 290.520\ \beta'$
			0.81	$K_{R,\mathrm{rel}} = 69.215\ \beta'$	3	1	83.3	0.24	$K_{R,\mathrm{rel}} = 150.830\ \beta'$
2	1		2.56	$K_{R,\mathrm{rel}} = 76.875\ \beta'$				1.22	$K_{R,\mathrm{rel}} = 161.260\ \beta'$
			6.25	$K_{R,\mathrm{rel}} = 85.875\ \beta'$				3.84	$K_{R,\mathrm{rel}} = 215.310\ \beta'$
		83.3	0.24	$K_{R,\mathrm{rel}} = 66.648\ \beta'$				9.38	$K_{R,\mathrm{rel}} = 321.250\ \beta'$
			1.22	$K_{R,\mathrm{rel}} = 69.801\ \beta'$					
2	1		3.84	$K_{R,\mathrm{rel}} = 76.944\ \beta'$					
			9.38	$K_{R,\mathrm{rel}} = 84.165\ \beta'$					

for different values of the aspect ratio (a/h), stiffener slenderness (s_s/a), and β values.

Several key observations can be made from the table:

(i) For an aspect ratio of $a/h = 1$, the relative rotational stiffness is minimally affected by the size of the flanges, irrespective of the load configuration and panel slenderness. This implies that the contribution of the stiffener to the rotational stiffness remains relatively constant for this aspect ratio.

(ii) For aspect ratios of $a/h = 2$ and 3, the values of $K_{R,\mathrm{rel}}$ exhibit significant variations depending on β' and β. This indicates that the impact of the stiffeners on the rotational stiffness becomes more pronounced as the aspect ratio increases. The characteristics of the two flanges influence the contribution of the stiffeners, leading to variations in the relative rotational stiffness.

5. Discussion

The following insights can be derived from the results:

The aspect ratio of the panel has a more significant influence on the relative rotational stiffness than the length of the

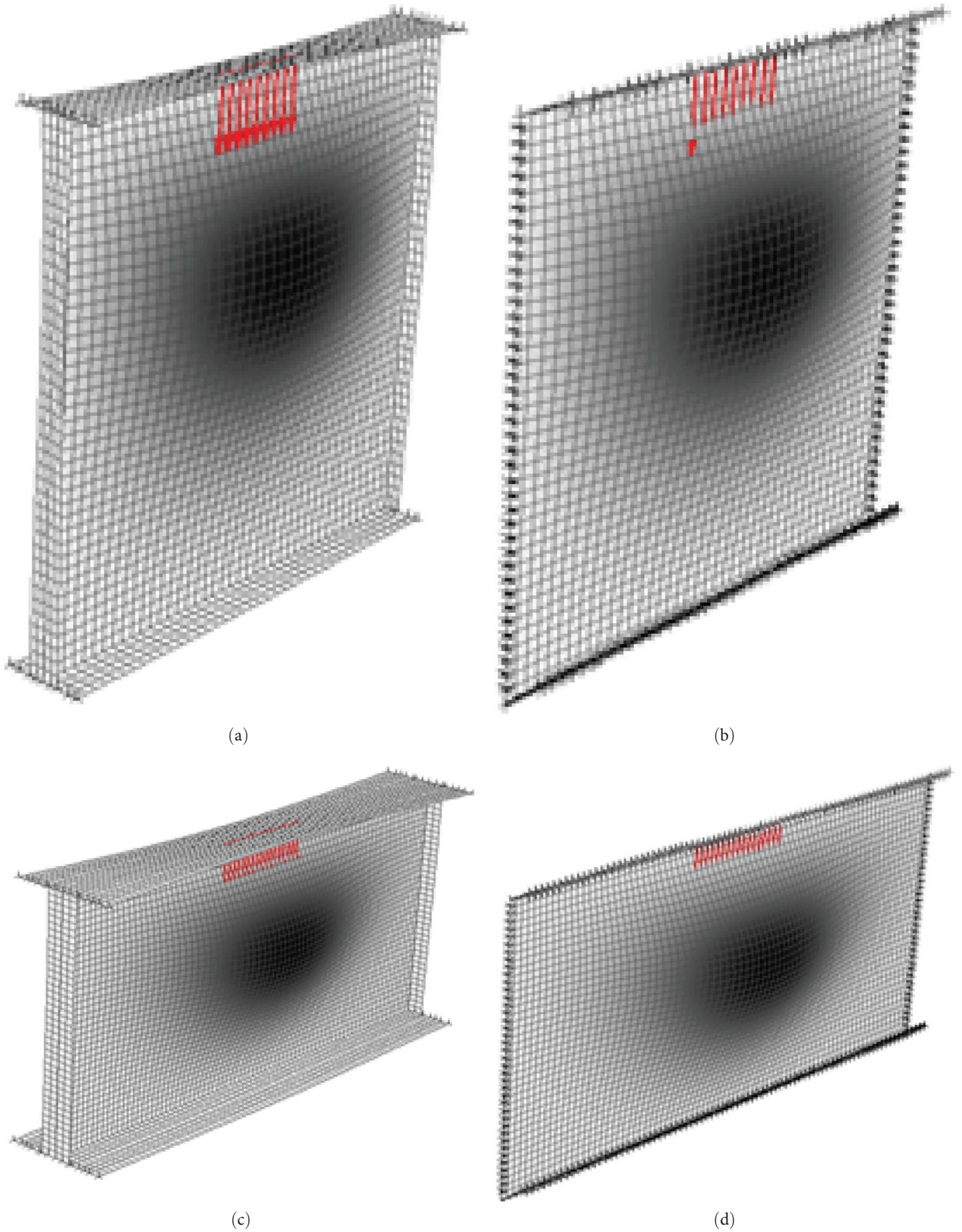

(a) (b) (c) (d)

Figure 8: Continued.

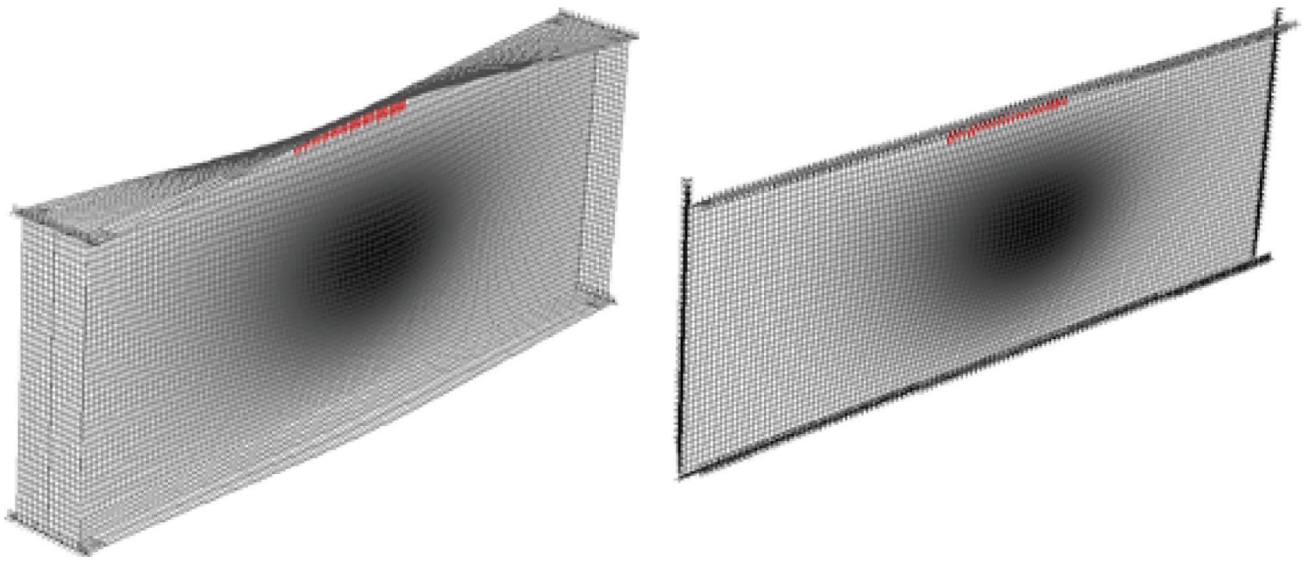

(e) (f)

Figure 8: Deformed configurations of 3d and 2d models.

applied load. This suggests that the geometric configuration of the panel plays a more significant role in determining the rotational stiffness behavior.

Holding other factors constant, the value of $K_{R,\text{rel}}$ tends to increase with an increase in the aspect ratio. This indicates that larger aspect ratios result in higher relative rotational stiffness, reflecting the enhanced rotational confinement provided by the stiffeners.

Based on these findings, it can be concluded that the size and configuration of the stiffeners and the panel's aspect ratio have a notable influence on the relative rotational stiffness.

It must be remarked that the regression analysis conducted to determine the relative rotational stiffness ($K_{R,\text{rel}}$) for the stiffeners exhibits excellent quality, making it meaningful to omit the reporting of error metrics. The obtained regression equations accurately capture the relationship between the input parameters (β', β) and the resulting relative rotational stiffness values. The high quality of the regressions is reflected in the consistency and reliability of the predicted $K_{R,\text{rel}}$ values across the different combinations of aspect ratio, stiffener slenderness, and β values.

Figure 8 illustrates several buckled configurations, and it is evident that the deformed panels exhibit qualitative similarities in both models.

It is worth noting that employing a nonlinear buckling analysis might enhance the validation of our results. Relying solely on the linear buckling analyses can be nonconservative, especially when addressing local instabilities. Drawing a comparison between the proposed method and a comprehensive nonlinear buckling analysis—which incorporates both material and geometric nonlinearities—would shed light on the considered buckling phenomena

5.1. Working Example. The working example presented in this section aims to demonstrate the application of a 2d plate model in determining the stiffness values of a structural system. The system under consideration consists of a panel constrained by stiffeners, and the rotational stiffness of the stiffeners is considered using rotational springs around the y-axis. In this example, we focus on a specific configuration with defined input variables such as the aspect ratio of the panel (a/h), the dimensions of the panel and stiffeners, and the slenderness ratio (s_s/a). These variables play a significant role in influencing the rotational stiffness of the stiffeners.

Following the prescribed procedure, which involves intermediate calculations based on the input variables, we determine the relative rotational and translational stiffness values for the upper and lower flanges and the stiffeners. The 2d plate model allows us to quantify the stiffness contributions of each component within the system. To validate the accuracy of the 2d plate model, a comparison is made with results obtained from a more detailed 3d model. The comparison helps assess the reliability of the simplified 2d approach in predicting the stiffness behavior of the system.

Overall, this working example is an illustrative case, demonstrating the application of the 2d plate model and highlighting the agreement between the 2d and 3d models' stiffness results.

Input variables:

(i) $a/h = 2$
(ii) $t = 12\,\text{mm}$
(iii) $t_1 = 24\,\text{mm}$
(iv) $b_1 = 480\,\text{mm}$
(v) $t_2 = 18\,\text{mm}$
(vi) $b_2 = 216\,\text{mm}$
(vii) $s_s/a = 0.2$
(viii) $\lambda = 83.333$

Intermediate calculations:

(i) $\beta = \frac{b_1 t_1^3}{ht^3} = 3.84$
(ii) $\gamma = \frac{b_1 t_1}{ht} = 0.96$
(iii) $\beta' = \frac{2b_2 t_2^3}{at^3} = 0.729$

Stiffness values:

(i) Upper flange relative rotational stiffness: $K_{R,\mathrm{rel},u} = 3.3450\beta' = 12.8448$ Nmm/rad
(ii) Lower flange relative rotational stiffness: $K_{R,\mathrm{rel},l} = 4.5440\beta' = 17.4489$ Nmm/rad
(iii) Upper flange relative translational stiffness: $K_{T,\mathrm{rel},u} = -0.44\gamma^2 + 3.364\gamma = 2.8239$ Nmm/rad
(iv) Lower flange relative translational stiffness: $K_{T,\mathrm{rel},l} = -0.348\gamma^2 + 2.627\gamma = 2.2012$ Nmm/rad

6. Conclusions

In the design of I-section beam webs for stability, it is customary to assume hinged boundary conditions along the panel's perimeter to ensure safety. However, the critical load values of the system exhibit significant variations depending on the relative stiffness of the edge restraints.

By analyzing the correlation between the relative translational stiffness ($K_{T,\mathrm{rel}}$) and dimensional axial stiffness (γ), as well as between the rotational stiffness ($K_{R,\mathrm{rel}}$) and adimensional bending stiffness (β and β') within the web/flanges/stiffeners system, it becomes possible to treat the web panels as 2d models confined by constraints with variable stiffness. This approach allows for substituting finite-rigidity constraints with elastically deformable translational and rotational elements, enabling a rapid determination of the spring constants.

Decoupling the translational and rotational restraints provides further insights into the behavior of plates subjected to patch loading. Based on the numerical results, the following conclusions can be drawn:

(i) When the load is distributed over the entire length (a) of the panel, the rotational contribution of the two flanges becomes more evenly distributed.
(ii) For a ratio of $a/h = 1$ and load values of $s_s/a = 0.2$ and 0.5, the upper flange exhibits higher relative stiffness than the lower flange. However, this trend is reversed when transitioning to a ratio of 1.
(iii) For ratios $a/h = 2$ and 3, the rotational stiffness around the upper flange decreases as the ratio (s_s/a) increases. On the other hand, the rotational stiffness of the lower flange decreases when transitioning from a load value of 0.2–0.5 but then increases between 0.5 and 1.

These findings contribute to a better understanding of the behavior of the web/flanges/stiffeners system under patch-loading conditions. By considering the variable stiffness constraints and their impact on the system, engineers can make more informed design decisions and ensure I-section beam webs' structural integrity and stability.

Nomenclature

a: Width of the web
b_1: Width of the flange
b_2: Width of the stiffener
Dx, Dy, Dz: Displacements in the x, y, z directions, respectively
E: Young's modulus of steel
F_{cr}: Elastic critical load
$F_{\mathrm{cr},i}$: Critical load at step i
i: Step number in the decoupling procedure
k_{cr}: Buckling coefficient
$k_{\mathrm{cr},i}$: Buckling coefficient at step i
K': Elastic stiffness per unit of spring length
K_R: Stiffness of rotational constraint
K_T: Stiffness of translational constraint
$K_{T,\mathrm{rel}}$: $\left(\frac{K_T}{E \cdot t}\right)$ Ratio between the adimensional translational stiffness and the axial stiffness of the plate. The subscripts u and l indicate the upper and lower flanges
h: Height of the web
K_R: Value of the rotational springs along the plate perimeter
K'_R: $\left(\frac{K_R \cdot n_{KR}}{a}\right)$ Rotational stiffness per unit of length
$K_{R,\mathrm{rel}}$: $\left(\frac{K_R \cdot n_{KR} \cdot 12(1-\nu^2) \cdot h_w}{E \cdot t^3 a}\right)$ Ratio between the adimensional rotational stiffness and the bending stiffness of the plate
n_{KR}: Number of nodes
Rx, Ry, Rz: Rotations about the x, y, z axes, respectively
s_s: Patch load length
t: Thickness of the 2d equivalent plate
t_1: Thickness of the flange
t_2: Thickness of the stiffener
x, y: Axes
β: $\left(\frac{b_1 t_1^3}{ht^3}\right)$ Ratio between rotational stiffness of flange and flexural rigidity of web panel
β': $\left(\frac{2b_2 t_2^3}{at^3}\right)$ Ratio between rotational stiffness of vertical stiffener and flexural rigidity of web panel
γ: $\left(\frac{b_1 t_1}{ht}\right)$ Adimensional geometric parameter
λ: Slenderness of the plate
λ_1: First eigenvalue of the stability problem
$\lambda_{1,i}$: Eigenvalue at step i
ν: Poisson's coefficient
σ_0: Compression stress in the plate.

Appendix

Validation of a 2d Fully Constrained Model

Based on the provided expressions, Tables 7–9 present a comprehensive comparison between the critical buckling loads ($k_{\mathrm{cr},3d}$) obtained using the proposed procedure and the corresponding values ($k_{\mathrm{cr},2d}$) obtained from a simplified 2d spring model in the case of the fully clamped plate. The tables facilitate a comparison of different parameters, including the

Table 7: Comparison between $k_{cr,3d}$ and $k_{cr,2d}$ spring following the proposed procedure for $a/h = 1$.

	$a/h=1$		$s_s/a=0.2$			$s_s/a=0.5$			$s_s/a=1$		
l	β	β'	$k_{cr,3d}$	$k_{cr,2d}$	$\frac{k_{cr,3d}}{k_{cr,2d}}$	$k_{cr,3d}$	$k_{cr,2d}$	$\frac{k_{cr,3d}}{k_{cr,2d}}$	$k_{cr,3d}$	$k_{cr,2d}$	$\frac{k_{cr,3d}}{k_{cr,2d}}$
		0.06	4.202	4.203	1.000	4.969	4.965	1.001	7.799	7.784	1.002
	0.08	0.08	4.256	4.240	1.004	5.043	5.016	1.005	7.931	7.874	1.007
		0.26	4.571	4.532	1.009	5.477	5.434	1.008	8.693	8.622	1.008
		0.06	5.633	5.591	1.008	6.596	6.551	1.007	10.243	10.182	1.006
	0.41	0.1	5.766	5.668	1.017	6.774	6.661	1.017	10.553	10.377	1.017
		0.32	6.171	6.006	1.027	7.332	7.157	1.024	11.532	11.274	1.023
		0.39	6.282	6.075	1.034	7.486	7.262	1.031	11.802	11.468	1.029
250		0.06	7.173	7.156	1.002	8.319	8.307	1.001	12.763	12.759	1.000
	1.28	0.1	7.303	7.249	1.007	8.493	8.433	1.007	13.065	12.976	1.007
		0.32	7.765	7.658	1.014	9.121	9.005	1.013	14.151	13.982	1.012
		0.49	7.995	7.810	1.024	9.437	9.226	1.023	14.699	14.381	1.022
		0.06	7.988	7.988	1.000	9.239	9.250	0.999	14.095	14.133	0.997
	3.13	0.1	8.117	8.089	1.003	9.410	9.384	1.003	14.390	14.360	1.002
		0.32	8.609	8.550	1.007	10.068	10.006	1.006	15.513	15.425	1.006
		0.49	8.836	8.758	1.009	10.378	10.251	1.012	16.050	15.856	1.012
		0.13	4.937	4.824	1.023	5.860	5.719	1.025	9.221	8.989	1.026
	0.16	0.15	5.034	4.877	1.032	5.992	5.797	1.034	9.452	9.130	1.035
		0.51	5.408	5.236	1.033	6.521	6.328	1.030	10.397	10.102	1.029
		0.13	6.887	6.778	1.016	8.059	7.935	1.016	12.484	12.299	1.015
	0.81	0.19	7.118	6.898	1.032	8.368	8.106	1.032	13.013	12.603	1.033
		0.65	7.615	7.317	1.041	9.064	8.730	1.038	14.249	13.743	1.037
		0.78	7.742	7.379	1.049	9.238	8.827	1.047	14.546	13.926	1.045
125		0.13	8.141	8.080	1.008	9.456	9.395	1.006	14.491	14.420	1.005
	2.56	0.19	8.353	8.222	1.016	9.738	9.587	1.016	14.973	14.750	1.015
		0.65	8.914	8.742	1.020	10.508	10.311	1.019	16.321	16.021	1.019
		0.97	9.135	8.883	1.028	10.809	10.515	1.028	16.845	16.390	1.028
		0.13	8.629	8.554	1.009	10.003	9.940	1.006	15.263	15.230	1.002
	6.25	0.19	8.833	8.703	1.015	10.274	10.145	1.013	15.722	15.566	1.010
		0.65	9.425	9.259	1.018	11.071	10.907	1.015	17.105	16.883	1.013
		0.97	9.631	9.414	1.023	11.355	11.127	1.020	17.605	17.274	1.019
		0.19	5.537	5.302	1.044	6.592	6.317	1.044	10.388	9.946	1.044
	0.24	0.23	5.664	5.360	1.057	6.765	6.408	1.056	10.686	10.110	1.057
		0.77	6.032	5.706	1.057	7.294	6.959	1.048	11.643	11.135	1.046
		0.19	7.630	7.448	1.024	8.933	8.722	1.024	13.825	13.508	1.023
	1.22	0.29	7.908	7.587	1.042	9.305	8.919	1.043	14.458	13.858	1.043
		0.97	8.402	8.024	1.047	10.000	9.569	1.045	15.703	15.047	1.044
		1.18	8.521	8.077	1.055	10.157	9.651	1.052	15.966	15.200	1.050
83.33		0.19	8.622	8.477	1.017	10.026	9.884	1.014	15.360	15.190	1.011
	3.84	0.29	8.871	8.637	1.027	10.358	10.102	1.025	15.925	15.563	1.023
		0.97	9.420	9.170	1.027	11.112	10.844	1.025	17.267	16.874	1.023
		1.46	9.596	9.280	1.034	11.351	11.010	1.031	17.684	17.174	1.030
		0.19	9.020	8.808	1.024	10.450	10.274	1.017	15.920	15.752	1.011
	9.38	0.29	9.264	8.973	1.032	10.770	10.496	1.026	16.462	16.141	1.020
		0.97	9.847	9.531	1.033	11.555	11.269	1.025	17.842	17.490	1.020
		1.46	10.009	9.654	1.037	11.777	11.446	1.029	18.233	17.806	1.024

Table 8: Comparison between $k_{cr,3d}$ and $k_{cr,2d}$ spring following the proposed procedure for $a/h = 2$.

	$a/h=2$		$s_s/a=0.2$			$s_s/a=0.5$			$s_s/a=1$		
l	β	β'	$k_{cr,3d}$	$k_{cr,2d}$	$\frac{k_{cr,3d}}{k_{cr,2d}}$	$k_{cr,3d}$	$k_{cr,2d}$	$\frac{k_{cr,3d}}{k_{cr,2d}}$	$k_{cr,3d}$	$k_{cr,2d}$	$\frac{k_{cr,3d}}{k_{cr,2d}}$
		0.03	2.803	2.847	0.985	3.48	3.54	0.983	5.624	5.719	0.983
	0.08	0.04	2.81	2.85	0.986	3.49	3.548	0.984	5.657	5.741	0.985
		0.13	2.854	2.884	0.990	3.58	3.619	0.988	5.858	5.925	0.989
		0.03	3.529	3.517	1.003	4.35	4.342	1.003	7.007	6.996	1.002
	0.41	0.05	3.546	3.523	1.007	4.39	4.357	1.006	7.082	7.039	1.006
		0.16	3.598	3.551	1.013	4.48	4.425	1.013	7.312	7.239	1.010
		0.2	3.614	3.557	1.016	4.51	4.44	1.016	7.378	7.282	1.013
250		0.03	4.705	4.679	1.006	5.82	5.792	1.005	9.35	9.316	1.004
	1.28	0.05	4.718	4.682	1.008	5.85	5.803	1.008	9.419	9.36	1.006
		0.16	4.762	4.699	1.013	5.93	5.857	1.013	9.648	9.553	1.010
		0.24	4.793	4.705	1.019	5.99	5.877	1.019	9.785	9.628	1.016
		0.03	5.904	5.885	1.003	7.35	7.33	1.003	11.78	11.76	1.002
	3.13	0.05	5.913	5.887	1.004	7.37	7.336	1.004	11.84	11.804	1.003
		0.16	5.94	5.897	1.007	7.43	7.379	1.007	12.05	11.996	1.004
		0.24	5.959	5.901	1.010	7.47	7.395	1.011	12.16	12.068	1.008
		0.06	3.075	3.076	1.000	3.82	3.817	1.000	6.19	6.183	1.001
	0.16	0.08	3.088	3.082	1.002	3.84	3.829	1.003	6.246	6.217	1.005
		0.26	3.142	3.123	1.006	3.94	3.918	1.006	6.486	6.452	1.005
		0.06	4.211	4.173	1.009	5.21	5.162	1.009	8.407	8.338	1.008
	0.81	0.1	4.242	4.18	1.015	5.27	5.181	1.016	8.538	8.401	1.016
		0.32	4.305	4.206	1.024	5.38	5.254	1.024	8.821	8.633	1.022
		0.39	4.328	4.211	1.028	5.42	5.266	1.029	8.909	8.672	1.027
125		0.06	5.676	5.635	1.007	7.06	7.012	1.007	11.36	11.301	1.005
	2.56	0.1	5.696	5.639	1.010	7.1	7.026	1.011	11.48	11.362	1.010
		0.32	5.741	5.654	1.015	7.2	7.08	1.016	11.74	11.582	1.014
		0.49	5.78	5.658	1.022	7.26	7.096	1.024	11.9	11.645	1.022
		0.06	6.712	6.682	1.004	8.38	8.355	1.003	13.45	13.428	1.001
	6.25	0.1	6.722	6.685	1.006	8.41	8.367	1.005	13.54	13.488	1.004
		0.32	6.746	6.695	1.008	8.47	8.412	1.007	13.77	13.7	1.005
		0.49	6.764	6.699	1.010	8.51	8.426	1.010	13.87	13.759	1.008
		0.1	3.292	3.267	1.008	4.09	4.055	1.009	6.658	6.588	1.011
	0.24	0.11	3.312	3.274	1.012	4.13	4.07	1.014	6.739	6.627	1.017
		0.39	3.368	3.315	1.016	4.23	4.162	1.016	6.978	6.874	1.015
		0.1	4.709	4.641	1.015	5.85	5.758	1.015	9.462	9.324	1.015
	1.22	0.14	4.752	4.647	1.023	5.92	5.778	1.025	9.639	9.392	1.026
		0.49	4.82	4.67	1.032	6.05	5.845	1.035	9.935	9.62	1.033
		0.59	4.85	4.673	1.038	6.1	5.855	1.041	10.04	9.652	1.040
83.33		0.1	6.201	6.145	1.009	7.74	7.679	1.008	12.47	12.392	1.006
	3.84	0.14	6.223	6.149	1.012	7.78	7.696	1.011	12.6	12.457	1.011
		0.49	6.264	6.162	1.017	7.87	7.746	1.016	12.85	12.671	1.014
		0.73	6.307	6.165	1.023	7.94	7.758	1.023	13.01	12.72	1.023
		0.1	7.06	7.007	1.008	8.82	8.787	1.003	14.16	14.144	1.001
	9.38	0.14	7.069	7.01	1.008	8.84	8.8	1.005	14.25	14.211	1.003
		0.49	7.09	7.02	1.010	8.9	8.843	1.006	14.46	14.415	1.003
		0.73	7.106	7.022	1.012	8.93	8.853	1.009	14.55	14.462	1.006

Table 9: Comparison between $k_{cr,3d}$ and $k_{cr,2d}$ spring following the proposed procedure for $a/h = 3$.

	$a/h=3$		$s_s/a=0.2$			$s_s/a=0.5$			$s_s/a=1$		
l	β	β'	$k_{cr,3d}$	$k_{cr,2d}$	$\frac{k_{cr,3d}}{k_{cr,2d}}$	$k_{cr,3d}$	$k_{cr,2d}$	$\frac{k_{cr,3d}}{k_{cr,2d}}$	$k_{cr,3d}$	$k_{cr,2d}$	$\frac{k_{cr,3d}}{k_{cr,2d}}$
		0.02	2.687	2.783	0.966	3.361	3.519	0.955	5.173	6.69	0.773
	0.08	0.03	2.69	2.783	0.967	3.371	3.52	0.958	5.199	6.698	0.776
		0.09	2.708	2.785	0.972	3.436	3.526	0.974	5.361	6.762	0.793
		0.02	3.35	3.349	1.000	4.49	4.513	0.995	7.452	7.582	0.983
	0.41	0.03	3.353	3.349	1.001	4.499	4.515	0.996	7.49	7.601	0.985
		0.11	3.362	3.35	1.004	4.525	4.523	1.000	7.601	7.684	0.989
		0.13	3.365	3.35	1.004	4.533	4.525	1.002	7.633	7.701	0.991
250		0.02	4.291	4.274	1.004	5.764	5.744	1.003	9.607	9.633	0.997
	1.28	0.03	4.294	4.274	1.005	5.772	5.744	1.005	9.642	9.652	0.999
		0.11	4.304	4.274	1.007	5.796	5.747	1.009	9.746	9.734	1.001
		0.16	4.312	4.274	1.009	5.815	5.749	1.011	9.814	9.764	1.005
		0.02	5.45	5.432	1.003	7.473	7.441	1.004	12.56	12.558	1.000
	3.13	0.03	5.452	5.432	1.004	7.478	7.442	1.005	12.59	12.58	1.000
		0.11	5.458	5.433	1.005	7.493	7.443	1.007	12.68	12.667	1.001
		0.16	5.464	5.433	1.006	7.506	7.443	1.008	12.73	12.696	1.003
		0.04	2.967	3.002	0.988	3.968	4.088	0.971	6.525	6.896	0.946
	0.16	0.05	2.969	3.002	0.989	3.977	4.089	0.973	6.561	6.909	0.950
		0.17	2.979	3.005	0.991	4.012	4.102	0.978	6.711	6.999	0.959
		0.04	3.866	3.854	1.003	5.168	5.159	1.002	8.626	8.671	0.995
	0.81	0.06	3.873	3.854	1.005	5.186	5.161	1.005	8.691	8.697	0.999
		0.22	3.887	3.855	1.008	5.219	5.167	1.010	8.82	8.789	1.004
		0.26	3.893	3.855	1.010	5.233	5.169	1.012	8.863	8.804	1.007
125		0.04	5.188	5.158	1.006	7.058	7.01	1.007	11.86	11.831	1.002
	2.56	0.06	5.194	5.159	1.007	7.071	7.011	1.009	11.92	11.858	1.005
		0.22	5.206	5.159	1.009	7.099	7.012	1.012	12.03	11.946	1.007
		0.32	5.22	5.159	1.012	7.129	7.013	1.017	12.13	11.97	1.013
		0.04	6.446	6.416	1.005	9.009	8.966	1.005	15.28	15.273	1.000
	6.25	0.06	6.448	6.416	1.005	9.014	8.967	1.005	15.32	15.304	1.001
		0.22	6.453	6.417	1.006	9.025	8.97	1.006	15.41	15.399	1.000
		0.32	6.46	6.417	1.007	9.041	8.97	1.008	15.47	15.421	1.003
		0.06	3.129	3.148	0.994	4.198	4.263	0.985	7.003	7.212	0.971
	0.24	0.08	3.132	3.148	0.995	4.208	4.265	0.987	7.043	7.228	0.974
		0.26	3.142	3.15	0.997	4.238	4.277	0.991	7.166	7.323	0.979
		0.06	4.259	4.229	1.007	5.713	5.667	1.008	9.577	9.551	1.003
	1.22	0.1	4.27	4.23	1.009	5.739	5.671	1.012	9.667	9.581	1.009
		0.32	4.288	4.23	1.014	5.779	5.676	1.018	9.805	9.669	1.014
		0.39	4.297	4.23	1.016	5.798	5.677	1.021	9.86	9.681	1.018
83.33		0.06	5.758	5.713	1.008	7.918	7.852	1.008	13.38	13.328	1.004
	3.84	0.1	5.765	5.713	1.009	7.933	7.852	1.010	13.45	13.355	1.007
		0.32	5.778	5.714	1.011	7.961	7.854	1.014	13.56	13.439	1.009
		0.49	5.798	5.714	1.015	8.002	7.855	1.019	13.68	13.456	1.016
		0.06	6.945	6.903	1.006	9.789	9.762	1.003	16.67	16.716	0.997
	9.38	0.1	6.947	6.903	1.006	9.793	9.763	1.003	16.71	16.747	0.998
		0.32	6.951	6.904	1.007	9.803	9.766	1.004	16.79	16.834	0.997
		0.49	6.96	6.904	1.008	9.82	9.766	1.006	16.84	16.848	1.000

ratio of web thickness to height (a/h) and the ratio of stiffener spacing to web spacing (s_s/a).

The comparison is presented in Table 7 for the fully constrained case where a/h is 1. The values of $k_{cr,3d}$ and $k_{cr,2d}$ are provided for various combinations of l, β, and β'. The results showcase the calculated critical buckling loads for both the 3d model and the 2d spring model. Specifically, the values of $k_{cr,3d}$ obtained from the proposed procedure are compared with those of $k_{cr,2d}$ obtained from the simplified 2d spring model.

Similarly, in Tables 8 and 9, the fully constrained comparison is presented for the case where a/h is 2 and 3, respectively.

For $a/h = 1$, the $k_{cr,3d}$ is greater than $k_{cr,2d}$. This indicates that the estimated 2d value is slightly underestimated. The relative percentage reduction is consistently below 6%. The peak errors, approximately 5%, are generally observed for larger values of β, particularly for the cases when $\lambda = 83.33$ with β values of 0.24 and 1.22. For $a/h = 2$, the relative reduction of the 2d buckling coefficient compared to the 3d is also minor, with the deviation never exceeding 5%. A variation of around 4% is noted for $\lambda = 83.33$ with $\beta = 1.22$. However, the scenario is different for $a/h = 3$. Here, the 2d coefficient overestimates the 3d value by approximately 20% in three instances, specifically for $\lambda = 250$, $\beta = 0.08$, and $ss/a = 1$. In other situations, the discrepancy is even less than in the previous cases, averaging below 2%.

Data Availability

All models or codes supporting this study's findings are available from the corresponding author upon request.

Conflicts of Interest

The authors declare that they have no conflicts of interest.

Acknowledgments

The author would like to express their gratitude to Mr E. Mazzocato for his valuable contributions to the numerical analyses conducted during the research for this thesis.

References

[1] S. C. Lee, C. H. Yoo, and D. Y. Yoon, "Behaviour of intermediate transverse stiffeners attached on web panels," *Journal of Structural Engineering*, vol. 128, no. 3, pp. 337–345, 2002.

[2] C. A. Graciano and B. Edlund, "Non-linear fe analysis of longitudinally stiffened girder webs under patch loading," *Journal of Constructional Steel Research*, vol. 58, no. 9, pp. 1231–1245, 2002.

[3] C. Graciano and O. Lagerqvist, "Critical buckling of longitudinally stiffened webs subjected to compressive edge loads," *Journal of Constructional Steel Research*, vol. 59, no. 9, pp. 1119–1146, 2003.

[4] M. Xie and J. C. Chapman, "Design of web stiffeners: local panel bending effects," *Journal of Constructional Steel Research*, vol. 60, no. 10, pp. 1425–1452, 2004.

[5] M. M. Alinia, "A study into optimization of stiffeners in plates subjected to shear loading," *Thin-Walled Structures*, vol. 43, no. 5, pp. 845–860, 2005.

[6] E. Maiorana, C. Pellegrino, and C. Modena, "Influence of longitudinal stiffeners on elastic stability of girder webs," *Journal of Constructional Steel Research*, vol. 67, no. 1, pp. 51–64, 2011.

[7] S. Timoshenko and S. Woinowsky-Krieger, *Theory of Plates and Shells*, McGraw-Hill Book Company, 1959.

[8] F. Shahabian and T. M. Roberts, "Buckling of slender web plates subjected to combinations of in-plane loading," *Journal of Constructional Steel Research*, vol. 51, no. 2, pp. 99–121, 1999.

[9] T. Porter, K. Rockey, and H. Evans, "The collapse behaviour of plate girders loaded in shear," *Structural Engineering*, vol. 53, no. 9, pp. 313–325, 1975.

[10] Z. Sadovský, A. P. Teixeira, and C. Guedes Soares, "Degradation of the compressive strength of rectangular plates due to initial deflection," *Thin-Walled Structures*, vol. 43, no. 1, pp. 65–82, 2005.

[11] P. Granath and O. Lagerqvist, "Shaped steel girders subjected to combined bending moment and travelling patch loading," *Journal of Constructional Steel Research*, vol. 55, pp. 153–181, 2000.

[12] E. Maiorana, C. Pellegrino, and C. Modena, "Imperfections in steel girders with and without perforations under patch loading," *Journal of Constructional Steel Research*, vol. 65, no. 5, pp. 1121–1129, 2009.

[13] V. T. Lian and N. E. Shanmugam, "Openings in horizontally curved plate girder webs," *Thin-Walled Structures*, vol. 41, no. 4, pp. 245–269, 2003.

[14] A. L. Yettram and C. J. Brown, "The elastic stability of square perforated plates under bi-axial loading," *Computers & Structures*, vol. 22, no. 4, pp. 589–594, 1986.

[15] M. A. Komur and M. Sonmez, "Elastic buckling of perforated plates with single and multiple circular openings," *Mechanics Research Communications*, vol. 35, no. 3, pp. 361–371, 2008.

[16] Z. Yang, C.-B. Kim, C. Cho, and H. G. Beom, "The concentration of stress and strain in finite thickness elastic plates containing a circular hole," *International Journal of Solids and Structures*, vol. 45, no. 3-4, pp. 713–731, 2008.

[17] T. Ren and G. S. Tong, "Elastic buckling of web plates in I-girders under patch and wheel loading," *Engineering Structures*, vol. 27, no. 10, pp. 1528–1536, 2005.

[18] M. Rogač, S. Aleksić, and D. Lučić, "Influence of patch load length on resistance of I-girders. Part-I: experimental research," *Journal of Constructional Steel Research*, vol. 175, Article ID 106369, 2020.

[19] M. I. M. Hesham Martini, "Elasto-plastic lateral torsional buckling of steel beams with perforated web," 2011.

[20] J. Gozzi, "Patch loading resistance of plated girders: ultimate and serviceability limit state," 2007.

[21] B. Kövesdi, B. Braun, U. Kuhlmann, and L. Dunai, "Patch loading resistance of girders with corrugated webs," *Journal of Constructional Steel Research*, vol. 66, no. 12, pp. 1445–1454, 2010.

[22] R. Chacón, J. Herrera, and L. Fargier-Gabaldón, "Improved design of transversally stiffened steel plate girders subjected to patch loading," *Engineering Structures*, vol. 150, pp. 774–785, 2017.

[23] S. Kovacevic, A. Ceranic, and N. Markovic, "Patch load resistance of longitudinally stiffened steel plate girders: a parametric study," *Ce/Papers–Proceedings in Civil Engineering*, vol. 4, no. 2–4, pp. 2107–2114, 2021.

[24] N. Loaiza, C. Graciano, R. Chacón, and E. Casanova, "16.20: Influence of bearing length on the patch loading resistance of multiple longitudinally stiffened webs," *Ce/Papers–Proceed-Proceedings in Civil Engineering*, vol. 1, no. 2-3, pp. 4199–4204, 2017.
[25] R. Chacón and R. Zorrilla, "Structural health monitoring in incrementally launched steel bridges: patch loading phenomena modeling," *Automation in Construction*, vol. 58, pp. 60–73, 2015.
[26] G+D Computing, Sydney, "Strand7 User's Manual," 2005.
[27] P. Granath and O. Lagerqvist, "Behaviour of girder webs subjected to patch loading," *Journal of Constructional Steel Research*, vol. 50, no. 1, pp. 49–69, 1999.
[28] S. Kovacevic and N. Markovic, "Experimental study on the influence of patch load length on steel plate girders," *Thin-Walled Structures*, vol. 151, Article ID 106733, 2020.